16 Light Scattering by Regular Particles on Flat Substrates

J.M. Saiz, J.L. de la Peña, P.J. Valle, F. González, and F. Moreno

Departamento de Física Aplicada. Grupo de Óptica.
Universidad de Cantabria. 39005 Santander. SPAIN.

Abstract. Light scattering intensity patterns produced by particles on substrates depend strongly on the size and shape of the particles. For some regular particle shapes, like spheres and cylinders, minima exist in the intensities and a relationship exists between their angular positions and the particle size. This dependence may be established using a simple double-interaction model which considers only the following: a) the scattering solution for the isolated particle; b) the coherent addition of four contributions of the scattering amplitudes to account for the field reflections off the substrate; and c) some geometrical factors which include the path differences, the Fresnel reflection coefficients, and the geometrical shadowing. This model has been used to size particles when illuminated at both normal and oblique incidence. For a collection of polydisperse particles on a substrate, scattering patterns can also produce very useful information; for instance, the visibility of the minima is directly related to the variance in size for low polydispersity samples. For large values of polydispersity (more than 30%), the width of the enhanced-backscattering peak can provide useful information.

1 Introduction

Scattering by microstructures on flat substrates constitutes an important field of interest, since it includes particles as contaminants on clean manufactured surfaces [1]. Much effort has been devoted to modeling the scattered light from these surfaces, including the analysis of different effects and the test of approximate numerical solutions [2,3]. Among these effects are multiple scattering and cross-polarization [4], evolution of backscattering [5], near-field effects [6], enhancement of the surface field [7], and surface plasmon generation [8,9]. The development of models and approximate solutions contributes to our knowledge of the connection between the characteristics of the particle as a diffuser and the scattering patterns obtained from it. For instance, light scattering from particles on surfaces may sometimes show enough specific information to allow a direct estimate of the particle size, therefore constituting a simple and non-invasive particle sizing method [10,11].

Several features exist in the scattering patterns that may help in the inverse problem. These depend on the particular sample of interest and on the experimental feasibility of the observable feature. An extensive use of theoretical models can assist in the analysis. The simplest method of analysis is the angular positions of the minima of certain scattering patterns, and

F. Moreno and F. González (Eds.): Lectures 1998, LNP 534, pp. 285–300, 2000.

this method is our choice for most of the cases presented in this chapter. A great variety of models have been developed to assist us in our study of particulate surface. To be useful, the model must be physically meaningful, accurate, reliable, adaptable to many experimental conditions, and fast. Our choice for satisfying these criteria is the double-interaction model which we develop in Sect. 2. Section 3 is devoted to the inverse problem as an important application of the model. First, the size dependence of the minima in the scattering patterns is discussed, and expressions are obtained to find the particle size from the S-copolarized scattering patterns. The effect of size distributions on the scattering patterns is discussed later.

2 Theory

2.1 Double-Interaction Model and Shadowing Effects

A simplified method of the scattering by an object (in our case a sphere or a cylinder) on a flat substrate may be constructed by means of the double-interaction model [12]. The scattering problem is divided into several isolated-particle scattering problems, as pictured in Fig. 1, whose solution can be calculated.

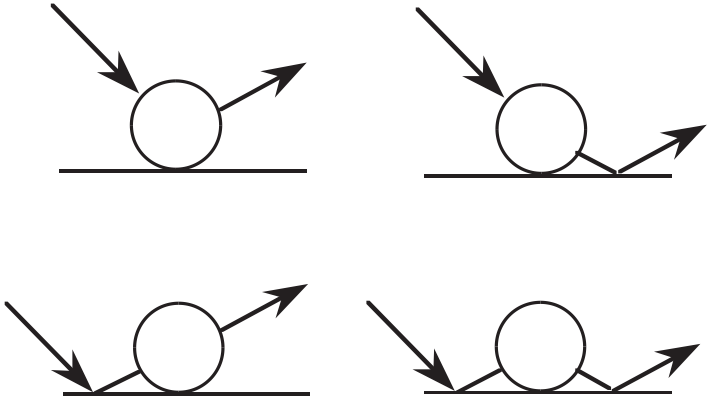

Fig. 1. Geometry of the double-interaction model. The superposition of these four components make up the total scattered electromagnetic field.

The particle of interest is centered a distance h above a flat substrate of complex refractive index m_{sub} and illuminated by a plane wave whose incident angle with respect to the surface normal is θ_i, taken always as positive, and wavelength λ. The spherical or cylindrical particles we consider are further characterized by their radius R and complex refractive index m_{par}. From Fig. 1, we see that the particle is actually illuminated by two different plane waves, directly and after a Fresnel reflection from the substrate. The particle then

scatters this incident light as if it were isolated. The light is scattered to a detector placed in the plane of incidence at observation angle θ_s. From Fig. 1, we see that the scattered light reaches the detector in two ways, one directly and the other after a Fresnel reflection from the substrate. There are four components to the total scattered field which we number as follows: 1) direct incident, direct scattered; 2) direct incident, reflected scattered; 3) reflected incident, direct scattered; and 4) reflected incident, reflected scattered. Note that this model does not include the multiple interactions that occur between the particle and the substrate.

Each of the four rays shown in Fig. 1 has traveled a different pathlength to reach the detector. Each pathlength results in one or more phase shifts $\delta(\theta)$ which depend on the incident angle or scattered angle ($\theta = \theta_i$ or θ_s), separation distance h, and wavelength, λ:

$$\delta(\theta) = \frac{4\pi h \cos\theta}{\lambda} \tag{1}$$

The amplitudes and phases are also modified by the Fresnel reflections occuring when the light rays reflect off the substrate:

$$\widehat{r}_s(\theta) = \frac{\cos\theta - \sqrt{m_{\text{sub}}^2 - \sin^2\theta}}{\cos\theta + \sqrt{m_{\text{sub}}^2 - \sin^2\theta}} \tag{2}$$

$$\widehat{r}_p(\theta) = -\frac{m_{\text{sub}}^2\cos\theta - \sqrt{m_{\text{sub}}^2 - \sin^2\theta}}{m_{\text{sub}}^2\cos\theta + \sqrt{m_{\text{sub}}^2 - \sin^2\theta}} \tag{3}$$

The four components of the total field may be written as follows:

$$E_1 = A_0\ A(\pi - \theta_i - \theta_s) \tag{4}$$

$$E_2 = A_0\ A(\theta_i - \theta_s)\widehat{r}_*(\theta_s)\ \exp\left[i\delta(\theta_s)\right] \tag{5}$$

$$E_3 = A_0\ A(\theta_i - \theta_s)\widehat{r}_*(\theta_i)\ \exp\left[i\delta(\theta_i)\right] \tag{6}$$

$$E_4 = A_0\ A(\pi - \theta_i - \theta_s)\widehat{r}_*(\theta_i)\ \widehat{r}_*(\theta_s)\exp\left[i\delta(\theta_i) + i\delta(\theta_s)\right] \tag{7}$$

where $\widehat{r}_*$ is the appropriate Fresnel reflection coefficient $\widehat{r}_s$ or $\widehat{r}_p$ depending on the polarization state of the incident or scattered ray; A_0 is the amplitude of the incident field; and $A(\theta)$ is the complex scattered field given by the isolated particle. For a spherical particle, $A(\theta)$ is the complex electric scattered field for an isolated sphere (Mie theory) at a scattering angle θ. The total scattered field is the superposition of these four components given by

$$E_T = \sum_{j=1}^{4} E_j \tag{8}$$

Equations (4-8) represent the double-interaction model in its purest form. Model results are fairly accurate and the equations can be evaluated almost as rapidly as the scattering results from the isolated particle. The only thing we have not considered in this model is the interaction which occurs between the particle and the substrate, i.e., the scattered waves from the particle that reflect of the substrate and are incident upon the particle. In the case of metallic particles, we can, however, make a first-order approximation of this effect by including the shadowing factors. Consider the third component E_3 when the incident angle approaches normal incidence $\theta_i \to 0°$. This component is obscured by the particle; i.e., the particle casts a shadow, hence a "shadowing effect" occurs for this component. Similarly, for the second component, the sphere obscures some of the light that reflects off the substrate when θ_s approaches zero. Both obscurations are present in the fourth contribution. To account for these effects, a shadowing factor $F_s(\theta)$ can be introduced on these components in the model. It is defined as the ratio between the shadowing cross-section (the obscured part) in the direction θ, where θ is either θ_i or θ_s and the total cross-section of the particle. For a sphere at rest on a substrate,

$$F_s(\theta) = 1 - \frac{2\,|\theta| + \sin|2\theta|}{\pi} \tag{9}$$

and for a cylinder

$$F_s(\theta) = 1 - \sin|\theta| \tag{10}$$

Including the shadowing factors, (4-7) become

$$E_1 = A_0\ A(\pi - \theta_i - \theta_s) \tag{11}$$

$$E_2 = A_0\ A(\theta_i - \theta_s)\widehat{r}_*(\theta_s)\ \exp\left[i\delta(\theta_s)\right]\left[1 - F_s(\theta_s)\right]^{\frac{1}{2}} \tag{12}$$

$$E_3 = A_0\ A(\theta_i - \theta_s)\widehat{r}_*(\theta_i)\ \exp\left[i\delta(\theta_i)\right]\left[1 - F_s(\theta_i)\right]^{\frac{1}{2}} \tag{13}$$

$$E_4 = A_0\ A(\pi - \theta_i - \theta_s)\widehat{r}_*(\theta_i)\ \widehat{r}_*(\theta_s)\exp\left[i\delta(\theta_s) + i\delta(\theta_s)\right] \times \left[1 - F_s(\theta_i)\right]^{\frac{1}{2}}\ \left[1 - F_s(\theta_s)\right]^{\frac{1}{2}} \tag{14}$$

It is interesting to emphasize the distinction between the radius of the particle and the distance from its center to the substrate surface. For the particle at rest on the substrate both are coincident but, for instance, the particle may be partially buried beneath the substrate interface and $h < R$. This is not uncommon experimentally when a sample is coated with a metallic layer. For such system, the size of the scatterer is not severely changed, but the phase shifts of contributions 2, 3 and 4 are decreased slightly [13]. The opposite case, $h > R$, occurs when a particle is lifted above a flat substrate. This is not uncommon for cylinders at rest on a flat substrate [14].

2.2 Model Accuracy

For many applications, approximate results are all that is necessary. The exact shapes and heights of the scattering intensity maxima and minima may not always be important. Many applications depend on the changes in the positions of the maxima and minima with system parameters. We demonstrate the accuracy of the double-interaction model in Fig. 2 which shows the scattering intensities as a function of scattering angle θ_s. For comparison, double-interaction results are shown with and without shadowing. Exact results are calculated using a method of images [14]. We see that the predictions achieved using the simple model agree quite well with the more complicated model. The inclusion of the shadowing effect improves the accuracy of the model results.

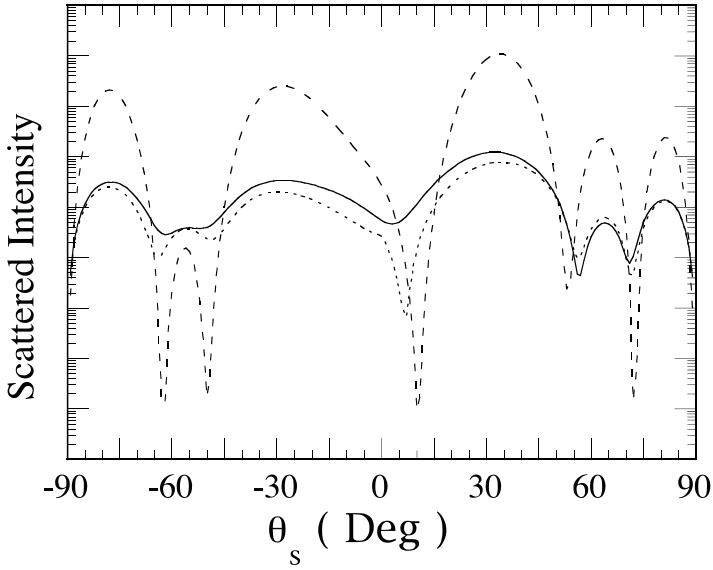

Fig. 2. Numerical s-polarized scattering patterns corresponding to an $R = 0.55$ μm cylinder on a substrate (both perfectly conducting) for $\theta_i = 30°$. Results are shown for the double-interaction model (solid), double-interaction model with shadowing effect (dotted), and exact results calculated using the method of [14] (dashed).

3 Application of the Model: A Particle Sizing Technique

The model presented above has two important characteristics: it is very fast, and it is reliable in reproducing the main properties of the scattering patterns. One of these properties, the position of the intensity minima, shows

clear regularities in its behavior when the size of the particle or the angle of incidence change. An extensive analysis has to be carried out in order to extract an analytic expression to characterize this behavior. Figure 3 shows the full-scan scattering pattern calculated by the model for S polarization within the plane of incidence for an $R = 0.55$ μm cylinder whose axis is perpendicular to that plane of incidence. The figure also shows the corresponding experimental results for such situation [11]. The positions of the intensity minima for the scattered light are approximately the same for the cylinder and sphere, although the scattering patterns are very different.

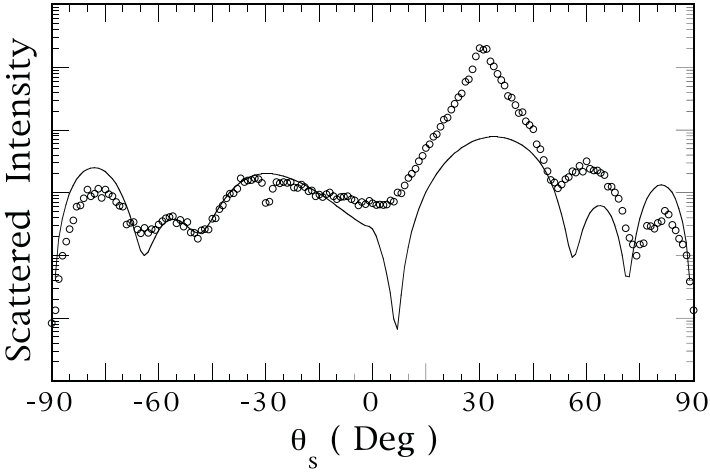

Fig. 3. Scattering pattern of an $R = 0.55$ μm cylinder on a substrate (both gold coated), $\theta_i = 30°$. Circles show experimental results and the continuous line shows double-interaction-model results including the shadowing effect.

3.1 Results: General Expression for Oblique Incidence

A particular scattering minimum can be represented by an index m. The order $m = 0$ corresponds to the minimum farthest from the specular peak (nearest grazing incidence). The order m increases towards the specular peak. Depending on the incident angle, there are two minima of each order on either side of the specular peak. To distinguish between these two sets, we refer to minima on the side of the specular peak including the back-scatter direction as the backward minima and those occuring on the other side of the specular peak as forward-scatter minima. Consequently, we define two scattering regions: the forward region, corresponding to $\theta_s > \theta_i$ and the backward region, corresponding to $\theta_s < \theta_i$. A great number of patterns similar to those of Fig. 3 have been calculated using the double-interaction model for different size parameters to study the behavior of the minima. Fig. 4 shows

one example of the minima for cylinders illuminated at $\theta_i = 20°$ plotted as a function of the inverse of the relative diameter $D_r = 2R \,/\, \lambda$.

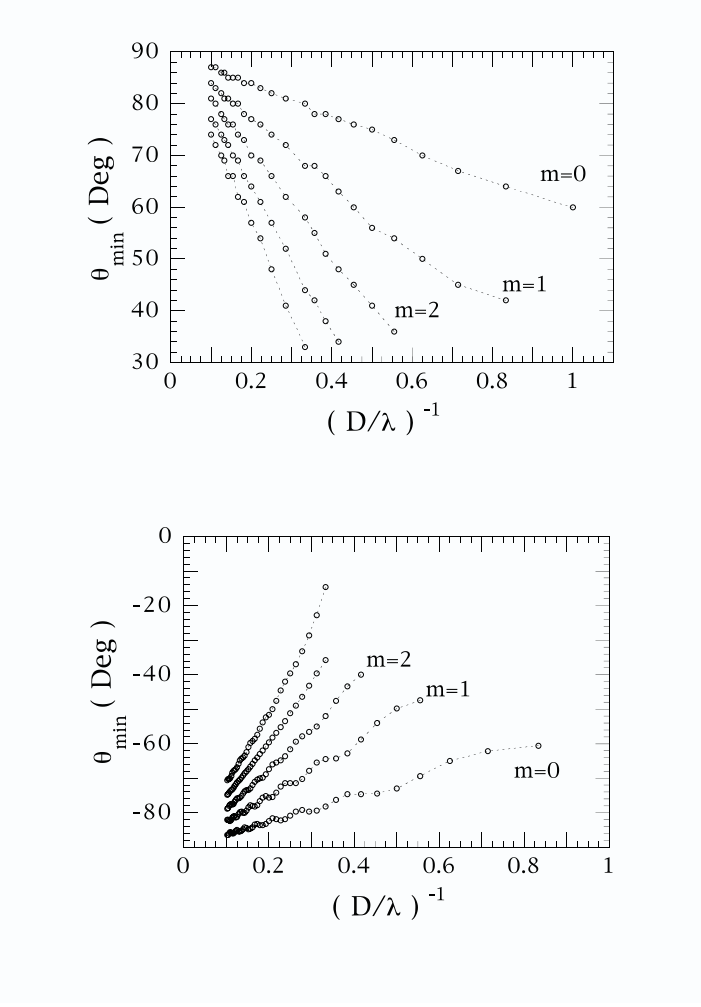

Fig. 4. Theoretical angular positions of minima for $\theta_i = 20°$ as a function of the relative diameter for cylinders on a substrate. The forward region ($\theta_s > \theta_i$) is shown on the top and the backward region ($\theta_s < \theta_i$) is shown on the bottom.

The behavior of the minima is approximately linear with $(D_r)^{-1}$. Plots for spheres are almost identical to those obtained for cylinders, meaning that, though the scattering patterns are different, the behavior of the minima are very similar. A general expression may be found relating the relative size to

the position of a minimum of order m. Forward and backward minima must be considered separately. The forward minima ($\theta > \theta_i$) can be described by

$$\theta_{\min} = 90 - \frac{\alpha_f}{D_r} \tag{15}$$

In the above equation, the position is inversely proportional to D_r, where

$$\alpha_f(\theta_i, m) = a(\theta_i) + b(\theta_i)m \tag{16}$$
$$a(\theta_i) = 33.47\,(\pm 0.08) - 0.097\,(\pm 0.010)\,\theta_i \tag{17}$$
$$b(\theta_i) = 36.40\,(\pm 0.05) - 0.149\,(\pm 0.006)\,\theta_i \tag{18}$$

Similarly, the backward minima ($\theta < \theta_i$) can be described by

$$\theta_{\min} = -90 + \frac{\alpha_b}{D_r} \tag{19}$$

where

$$\alpha_b(\theta_i, m) = a'(\theta_i) + b'(\theta_i)m \tag{20}$$
$$a'(\theta_i) = 33.55\,(\pm 0.08) + 0.153\,(\pm 0.010)\,\theta_i \tag{21}$$
$$b'(\theta_i) = 36.22\,(\pm 0.06) + 0.170\,(\pm 0.007)\,\theta_i \tag{22}$$

Obviously, $\theta_{\min} > \theta_i$ in the first case, and $\theta_{\min} < \theta_i$ in the second. Both $\theta_{\min}$ and θ_i are expressed in degrees. These expressions generalize that of [10] in which normal-incident illumination is considered. An evaluation of D_r (and

Table 1. Values of D (5th column) obtained from the experimental patterns, corresponding to particles of approximate nominal size D_{th}. N is the number of minima used in the fitting process. ΔD is the standard deviation, expressed in percent error in the last column.

Type	$D_{\text{th}}(\mu\text{m})$	θ_i(**Deg**)	N	$D(\mu\text{m})$	ΔD	%
Cylinder	1.1	0	4	**1.11**	0.07	(6.3)
		10	4	**1.07**	0.07	(6.5)
		20	4	**1.10**	0.08	(7.3)
		30	3	**1.08**	0.09	(8.3)
Sphere	1.1	8	4	**1.12**	0.08	(7.1)
		30	3	**1.13**	0.09	(8.0)
Sphere	3.2	8	16	**3.13**	0.27	(8.6)
		30	10	**3.19**	0.38	(12)

$D = D_r\lambda$) has been made by means of (15) and (19) for several samples. The angular positions of the minima have been obtained experimentally from the full-scan scattering patterns similar to those shown in Fig. 3, with an angular resolution of 1°. Table 1 shows the values obtained from measurements at different angles of incidence.

This particle-sizing method is simple, but often not accurate for many applications (see, for instance, [17]). However, the possibilities of the method have not been exploited yet, as we will see in the next subsection, where another procedure is described.

3.2 Tracking the Minima

The positions of the minima predicted by the model are almost coincident to those predicted by an exact solution (see Fig. 2) from normal incidence out to approximately $\theta_i = 30°$. This allows us to track the position of a minimum as the angle of incidence changes, and then compare the experimental evolution with that predicted by the model. The process is quite simple, avoiding the measurement of the full scattering patterns, and increasing the amount of information concerning that minimum. Once the scattering minima have been located for a given angle of incidence (usually normal incidence), one of these minima is selected, and the detecting system continuously scans a small interval around it. As the angle of incidence changes, the system tracks the minimum, obtaining a curve $\theta_{\min}(m)$ versus θ_i. This process can be carried out for any minima having measurable visibility.

Table 2. Values of D obtained from the experimental patterns, corresponding to particles of approximate nominal size $D_{\rm th}$. m corresponds to the order of the minimum which position has been fitted, either to the predictions of the model or to a linear behavior which cut at $\theta_i = 0°$ also serves the purpose of giving an estimate of D. The letter after the order stands for the forward (f) or the backward (b) minimum of order m. The interval in which the fit has been carried out is also specified.

Type	$\mathbf{D_{th}}$	**m**	*Interval* $[Deg, Deg]$	$\mathbf{D}(\mu\mathrm{m})$	$\Delta\mathbf{D}(\%)$
Model fit	1.1	1f	[0,16]	**1.079**	0.005 (0.5)
Model fit	1.1	1b	[0,20]	**1.077**	0.004 (0.4)
Linear $\theta_i = 0°$	1.1	1f	[0,12]	**1.072**	0.005 (0.5)
Linear $\theta_i = 0°$	1.1	1b	[0,12]	**1.071**	0.004 (0.4)

Two of these curves are shown in Fig. 5 for the case of a cylinder of approximate size $D = 1.1$ μm. The corresponding fit values are shown in the first part of Table 2. The use of the model may be minimized combining this

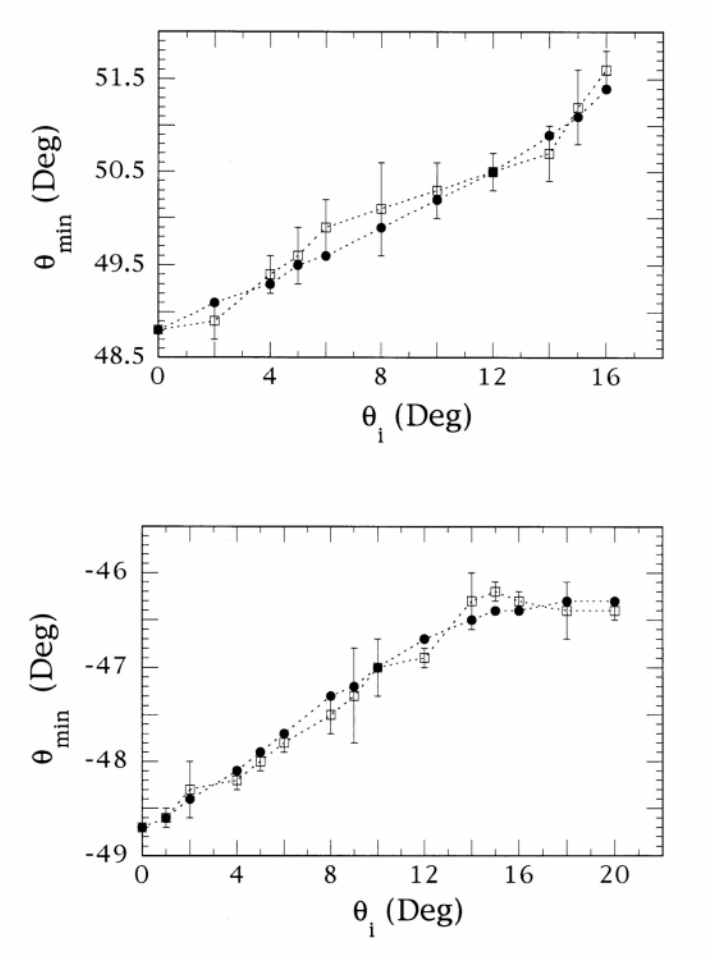

Fig. 5. Experimental (squares) and model (dots) predictions of the minima positions of order $m = 1$ as a function of the incident angle for a $D = 1.1$ μm cylinder. The forward region is shown on the top and backward region on the bottom.

procedure with the use of (15) and (19). These curves $\{\theta_{\min}/\theta_i\}$ have always a linear behavior up to about $\approx 10°$. We may obtain an accurate value of $\theta_{\min}$ for normal incidence by means of a linear fit. The size will be obtained by direct substitution in (15) and (19) – the result of this procedure is shown in the second part of Table 2.

3.3 Polydisperse Samples

Polydisperse samples contain particles having different properties. Most commonly, we consider a sample of particles having polydispersity in size, for instance, a distribution of spheres of identical material whose radii vary. Such samples are common in nature and in manufactured processes. We discuss methods of analysis of the scattering intensities from samples displaying high and low size polydispersities. These two different polydispersities require different analyses. We characterize the polydispersity by a gamma-type distribution because of its versatility

$$p(R, \mu, a)dR = \frac{R\mu^{-1}a^{\mu}\exp(-aR)}{\Gamma(\mu)}dR \tag{23}$$

with

$$a = \frac{R_o}{\sigma^2}; \qquad \mu = \frac{R_o^2}{\sigma^2} \tag{24}$$

and R_o is the mean radius of the particle and σ^2 the size variance. We also define the degree of polydispersity as

$$r = \mu^{-\frac{1}{2}} = \frac{\sigma}{R_o} \tag{25}$$

Low Polydispersity Distributions with $r < 0.1$ are considered here as having low polydispersity. These include, for example, samples of well characterized particles supplied by manufacturers. Another polydisperse sample may include a fiber whose radius varies along its length. In Fig.6 the model calculations of a scattering pattern corresponding to a monodisperse sample of spherical particles is compared with those of samples having different degrees of polydispersity. The immediate and obvious effect that a size distribution has on the scattering patterns is the loss of visibility in the pattern. This is due to the fact that different size microstructures have their minima at different angular positions. The incoherent addition of these scattering patterns causes a loss of visibility in the total measured scattering pattern. For high size polydispersity, the scattering patterns eventually lose all lobed structure.

In Fig. 6, the lobed pattern is still visible because of the relatively low degree of polydispersity. One very interesting feature is that the angular positions of the minima are approximately the same as those of the corresponding monodisperse system whose radius is the mean of the polydisperse sample. It can also be observed that the minima of higher order lose their visibility for lower polydispersities, while the lower orders still remain visible for not so

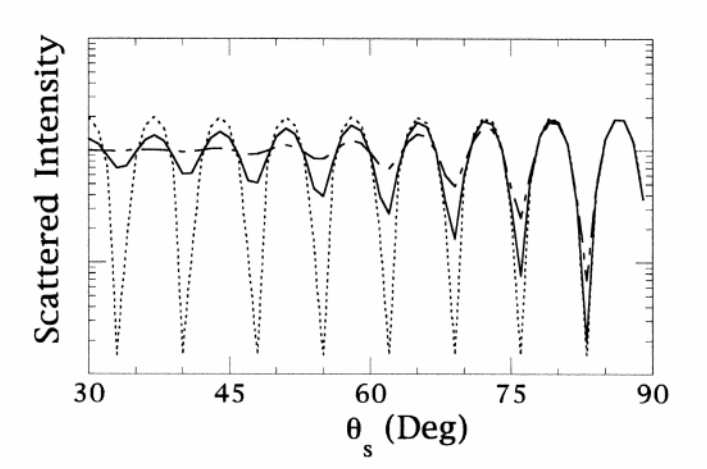

Fig. 6. Light scattering intensities from polydisperse spherical particles on a substrate illuminated at normal incidence as predicted by the double-interaction model including shadowing effects. The mean relative value is $R_{o,r} = R_o/\lambda = 2.53$ and $r = 0\%$ (dots), $r = 3\%$ (solid) and $r = 6\%$ (dashed) are shown.

low polydispersities. In Fig. 7 the evolution of the visibility as a function of the degree of polydispersity is plotted for several orders. In principle, a knowledge of the visibility for each order minima allows an estimate of the degree of polydispersity to be made. This, added to the fact that it is still possible to determine the central monodisperse value by means of the positions of the minima, leads to a characterization of the sample. In particular, Fig. 7 also shows the experimental data obtained from a cylinder of 1.1 μm diameter showing a nominal polidispersity of about 4% and illuminated along 2.5 mm.

High Polydispersity and Enhanced Back-Scattering For high polydispersity $r > 0.25$ the lobes in the scattering pattern become completely smoothed and can no longer be used to characterize the scattering system. To quantify the scattering system, we must resort to other methods. One useful method tool is the enhanced-backscatter peak. This is a coherent effect whose origin can be found in the superposition of the components described in Sect. 2. In the back-scattering direction, contributions of the once-reflected beams (components 2 and 3) always add constructively. This generally results in a peak in the back-scatter direction. High polydispersity helps to smooth out any remaining structure, so that the enhanced-backscatter peak is the only significant structure remaining. The width of this peak is inversely proportional to the size of any characteristic surface structures, and can be used to partially characterize the sample. The peak width is not only dependent on

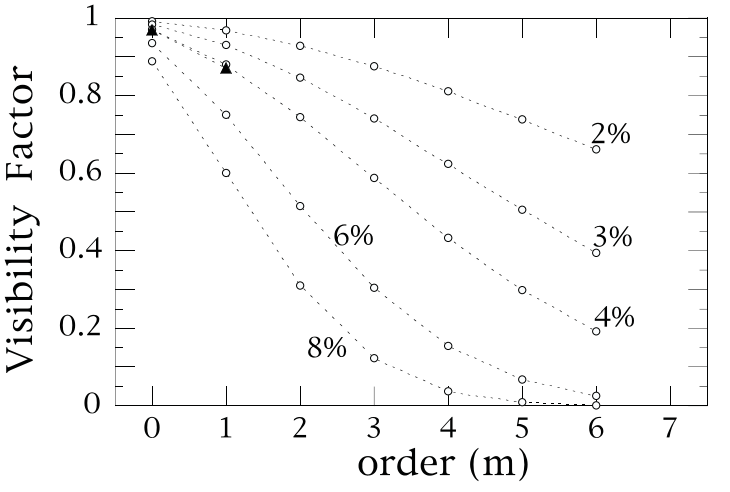

Fig. 7. Evolution of the visibility $V(m)$ for some values of r (expressed in %). Circles correspond to the measurable points (m=integer number). Dots lines with circles: Results predicted from the model. Dots lines with triangles: Experimental results for a Cylinder of approximate diameter $D = 1.1$ μm showing a polydispersity of about 4%.

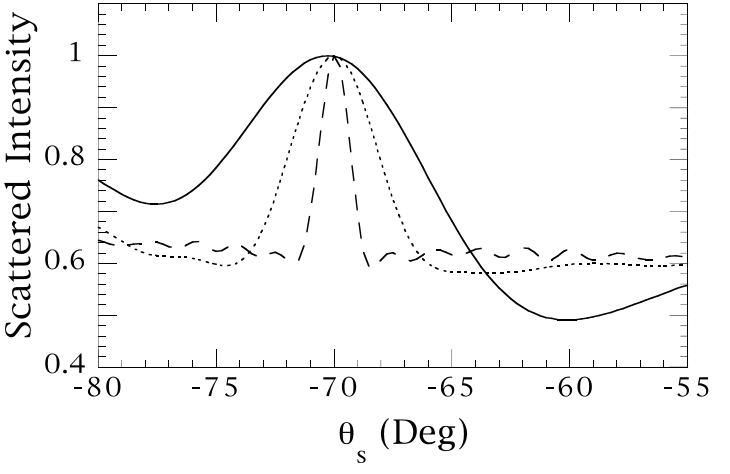

Fig. 8. Shape of the enhanced-back-scatter peak predicted by the model, for a sample of gold spherical particles of relative mean radius $R_{o,r} = R_o/\lambda = 1$ illuminated at $\theta_i = 70°$. Polydispersities of $r = 0.5$ (continuous line), $r = 1$ (dots line), and $r = 2$ (dashed line) are shown.

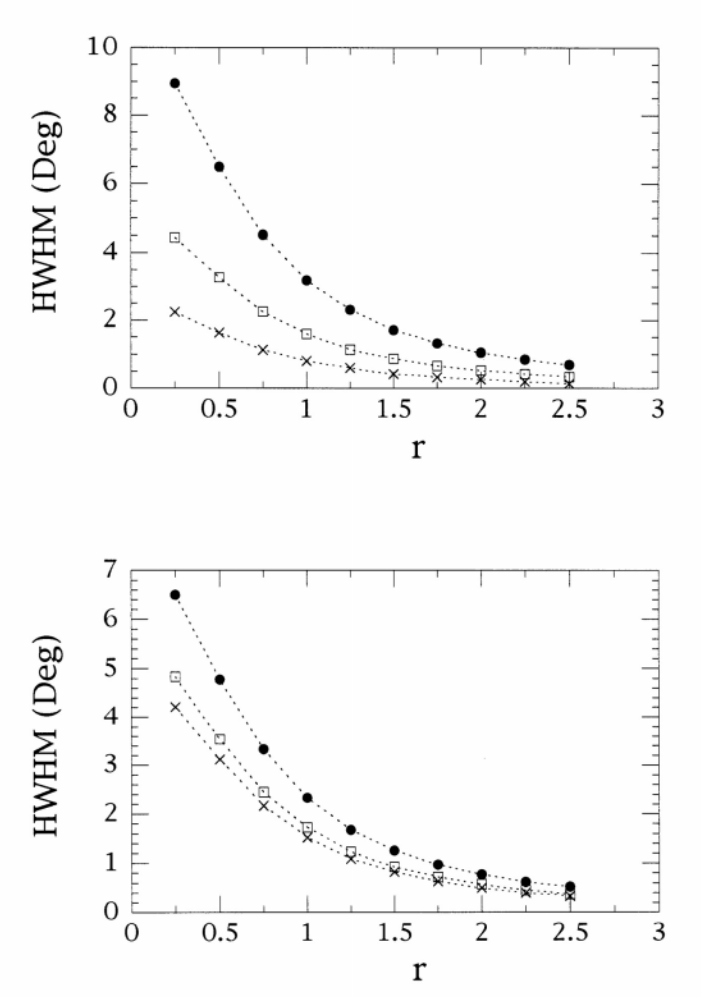

Fig. 9. Evolution of the back-scattering peak width as a function of polydispersity r. The top graph shows samples of $R_{o,r} = 0.5$ (dots), $R_{o,r} = 1$ (squares), and $R_{o,r} = 2$ (crosses) illuminated at $\theta_i = 70°$. The bottom graph shows samples of $R_{o,r} = 1$ illuminated at $\theta_i = 40°$ (dots), $\theta_i = 60°$ (squares), and $\theta_i = 80°$ (crosses).

the polydispersity, but also on the mean size and angle of incidence. Figure 8 shows the different shapes of the backscattering peak for different values of the degree of polydispersity r for $\theta_i = 70°$ and $R_o/\lambda = 1$. The width increases and the symmetry of the peak decreases as the value of r grows. In Fig. 9 the width is represented as a function of r and θ_i.

The fact that several combinations of r and $R_{o,r}$ produce the same peak width introduces an uncertainty in the determination of the mean size from the measurement of the width. In particular, a group of distributions with a constant product $rR_{o,r}$ produces approximately the same peak width. By itself, the experimental detection of a peak only provides information about which member of the family $rR_{o,r}$ the microstructures correspond.

4 Conclusions

The light scattered from a particle on a flat substrate may be approximately calculated from the knowledge of the scattering from the isolated particle. The double-interaction model is useful because of its simplicity, transparency, and speed at which it can be used to calculate and estimate properties of the particle system. Using this model, simple relationships can be established between scattering minima positions and contaminant size. The interference pattern has its origin in the particle uniformity, and a size polydispersity produces a progressive loss of visibility in the interference, which eventually completely destroys the lobed pattern. For the case of high polydispersity, the constructive interference of two of the components in the back-scatter direction allows us to make a quantitative measure of the scattering system. Although these principles have been applied to spherical and cylindrical metallic particles, the double-interaction method may be applied to other scattering systems. The characteristic evolution of the back-scattering patterns, the study of the out-of-plane scattered light, and the comparison between size and shape polydispersity for irregular particles are some of the applications for which this simple method may be applied.

5 Acknowledgments

The authors wish to thank the Dirección General de Enseñanza Superior for its financial support (project PB97-0345). J.L. de la Peña wishes to thank the Ministerio de Educación y Ciencia for his FPI grant. The authors wish also to thank Gorden Videen for his valuable comments.

References

1. B.M. Nebeker, G.W. Starr and E.D. Hirleman (1996), Evaluation of iteration methods used when modeling scattering from features on surfaces using the discrete-dipole approximation, J. Quant. Spectrosc. Radiat. Transfer **60**: 493
2. P.J. Valle, F. Moreno, J.M. Saiz, and F. González (1996), Electromagnetic interaction between two parallel circular cylinders on a planar interface, IEEE Trans. Antennas Propag. **44**: 321
3. Videen, G. (1991), Light scattering from a sphere on or near a plane substrate, J. Opt. Soc. Am. A **8**:483; Errata (1992), J. Opt. Soc. Am. A **9**:844
4. F. González, J.M. Saiz, P.J. Valle, and F. Moreno (1997), Multiple scattering in particulate surfaces: cross-polarization ratios and shadowing effects, Opt. Comm. **137**: 359
5. J.M. Saiz, P.J. Valle, F. González, F. Moreno, and D.L. Jordan (1994), Backscattering from particulate surfaces: experiment and theoretical modeling, Opt. Eng. **33**: 1261
6. A. Madrazo, and M. Nieto-Vesperinas (1995), Scattering of electromagnetic waves from a cylinder in front of a conducting plane, J. Opt. Soc. Am. A **12**: 1298
7. E.M. Ortiz, P.J. Valle, J.M. Saiz, F. González and F. Moreno (1998), A detailed study of the scattered near field of nanoprotuberances on flat surfaces, J. Phys. D: Appl. Phys. **31**: 3009
8. J.A. Sanchez-Gil (1998), Surface defect scattering of surface plasmon polaritons: Mirrors and light-emitters, Appl. Phys. Lett. **73**: 3509
9. A. Madrazo and M. Nieto-Vesperinas (1996), Surface structure and polariton interactions in the scattering of electromagnetic waves from a cylinder in front of a conducting grating: theory for the reflection phonon scanning tunneling microscope, J. Opt. Soc. Am. A **13**: 785
10. F. Moreno, J.M. Saiz, P.J. Valle, and F. González (1996), Metallic particle sizing on flat surfaces: Application to conducting substrates, Appl. Phys. Lett. **68**: 3087
11. J.L. de la Peña, F. González, J.M. Saiz, F. Moreno, and P.J. Valle (1999), Sizing particles on substrates: A general method for oblique incidence, Jour. Appl. Phys. **85**: 432
12. K.B. Nahm, and W.L. Wolfe (1987), Light scattering models for spheres on a conducting plane: comparison with experiment, Appl. Opt. **26**: 2995
13. J.M. Saiz, P.J. Valle, F. González, E.M. Ortiz, and F. Moreno (1996), Scattering by a metallic cylinder on a substrate: burying effects, Opt. Lett. **21**: 1330
14. Videen, G., Ngo, D. (1997), Light scattering from a cylinder near a plane interface: theory and comparison with experimental data, J. Opt. Soc. Am. A **14**:70
15. Nieto-Vesperinas M. (1991), Scattering and diffraction in physical optics. Wiley, New York.
16. J.M. Saiz, F. González, F. Moreno, and P.J. Valle (1995), Application of a ray-tracing model to the study of back scattering from surfaces with particles, J. Phys. D: Appl. Phys. **28**: 1040
17. B.W. Bell, and W.S. Bickel (1981), Single fiber light scattering matrix: An experimental determination, Appl. Opt. **20**: 3874